High Precision Measurements of the Permittivity of Water in the Microwave Range

H. J. Steinhoff, A. Redhardt, K. Lieutenant, W. Chrost, G. Hess, J. Schlitter,
and H. J. Neumann

Institut für Biophysik, Ruhr-Universität Bochum, 4630 Bochum, FRG

A practical version of a homodyne method for measuring the complex permittivity of high loss liquids at 3 and 9 GHz is described. The systematic errors are discussed in detail, because the homodyne method seems to be suitable as a simple standard method for precise measurements. The results of measurements on water in the temperature range 6 °C–45 °C are presented. The determination of all five parameters of the Debye function is possible. Finally, accuracy limiting factors for the determination of the relaxation parameters are discussed in detail.

Introduction

Corresponding to the outstanding importance of water in all natural sciences, the complex dielectric constant ε^* of this substance has been measured by many authors in a wide range of frequency and temperature; for a review see the contributions of Pottel et al. [1] or Hasted [2, 3].

The complete data set available in 1981 for ε^* as a function of temperature and frequency has been used by Kaatze and Uhlendorf to determine the parameters of the underlying dielectric relaxation [4]. The classical relaxation function of Cole [5] turned out to describe the experiments well.

Further examinations have shown that with the underlying accuracy of the measurements (typically 0.5% in the microwave range), many interesting details of the water relaxation cannot be resolved, as for example the distribution parameter α or the temperature dependence of the important high frequency limit ε_∞ of ε^* [6, 7, 8].

On the other hand, precise infrared methods are now available for the determination of the complex refractive index n^*. These measurements were carried out by Hasted et al. [9] and interpreted in terms of a Cole-function [5], to determine $\varepsilon_\infty(T)$. The results of these measurements differ from those obtained by dielectric methods. The difference is significant even at 25 °C, where ε^*-values can be determined with high accuracy [4, 6].

This gap has now to be closed from the side of ε^*-measurements. The introduction of new, precise measuring methods seems to be necessary [2]. So

Buckmaster and coworkers introduced a method for the determination of ε^* of high loss liquids in the microwave range [10–14], which uses an oversized waveguide transmission cell and a heterodyne detection. In a preceeding paper [15], we developed the basis of an alternative method, which uses small waveguides as measuring cells and a homodyne detection. The main points of [15] are

a) to show that the separation of higher waveguide modes, necessary for precise measurements, is possible,

b) the introduction of a homodyne method for ε^*-measurements,

c) the introduction of a numerical method for the investigation of systematic errors.

In the following we describe practical versions of the homodyne method at 3 and 9 GHz and discuss the systematic errors occuring in these set-ups. Finally, results of measurements on water are presented.

Experimental

Figure 1 shows the block diagram, which is identical in the essential points for both the 9 and 3 GHz apparatus built here. For both experiments reflex klystrons (X 13; 2K28) are used. Power is delivered by a highly stabilized hp 616 power supply, the klystrons are tempered by an oil bath so that the frequency drift is less than 3 kHz during the time required for a measurement – about 5 min.

As shown in Fig. 1 of [15], the microwave voltage incident on the diode is vectorially composed of a signal voltage U_S, containing the measuring information, and a reference voltage U_R, which is constant in phase and amplitude during a measurement.
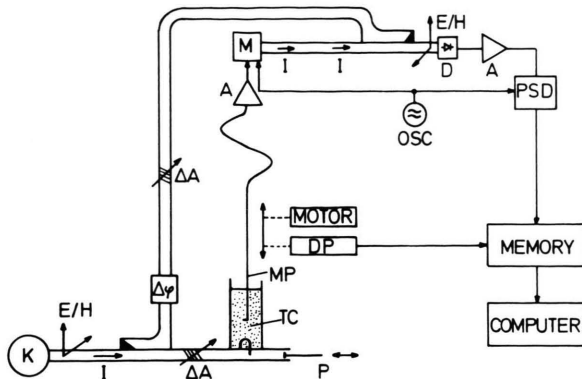
Fig. 1. Block diagram of the experimental set-up (X-band). (K), klystron; (E/H), E-H turner; (I), isolator; (ΔA), variable attenuator; ($\Delta\phi$), variable phase shifter; (P), movable plunger; (TC), transmission cell R 500 for X-band, R 320 for S-band, containing the liquid under test (for details see Fig. 2); (MP), movable probe; (A), amplifier; (M), modulator; (D), diode; (PSD), phase sensitive detector; (OSC), low frequency oscillator 50 kHz; (DP), displacement pick-up. X-band and S-band set up are identical in the electronic components. The waveguides are replaced by semi rigid cable in the S-band.

Fig. 2. Sectional drawing of the transmission measuring cell for the X-band. (1), X-band waveguide; (2), movable plunger for matching the *E*-field antenna; (3), adjustable *E*-field antenna; (4), coupling loop; (5) waveguide R 500, containing the liquid sample under test; (6), coupling loop, sensing the local *H*-field in the sample; (7), coaxial semirigid cable SR 06, feeding microwave signal to the receiver; (8), sliding copper block, supporting the semirigid cable; (9), microwave output to the receiver; (10) teflon insulators; (11), brass block in thermal contact with (5); (12), water tempering.

Signal Voltage

The main part of the microwave power (~ 100 mW) delivered by the klystron is fed into a vertically mounted waveguide, which serves as a transmission measuring cell (X-Band: R 500, 12.9 cm length, S-Band: R 320, 38 cm length), which is filled with the liquid under test. A matching network feeds the powder into the measuring cell by a coupling loop in such a way that even numbered TE_{0n}-modes are suppressed. The microwave field, travelling in this wave guide measuring cell, is detected by a movable probe (Fig. 2) and is led through an elastic, concentric semirigid cable SR 06 to a low noise microwave preamplifier. The amplified signal is modulated by a pin diode (50 kHz) and reaches the microwave diode, where it causes the signal voltage U_S. The isolators prevent back modulation of the reference voltage, which would give rise to undesired large zero displacements. Residual displacements are contained in V_0, Eq. 2 of [15], and can be accounted for.

Referenceg Voltage U_R

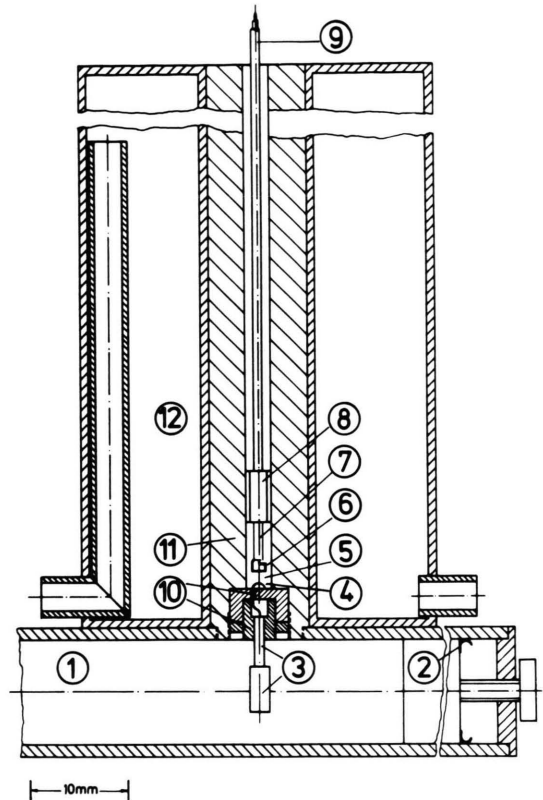To generate a reference voltage U_R, a part of the klystron power is fed into the diode using a branch-

line, which consists of an attenuator and a phase shifter. The attenuator and the phase shifter need not to be calibrated; they are adjusted once and remain unchanged during a measurement.

Signal Processing

In this way, the microwave voltage $U_R + U_S$ at the diode is composed of a large, unmodulated and constant reference voltage U_R and a small (50 kHz) amplitude modulated signal voltage U_S, whose phase and amplitude varies during the probe displacement.

After demodulation at the diode D, the amplitude $V_S(\zeta)$ of a 50 kHz-signal contains all the information

leading to ε^*. Hereby the amplitude of this signal varies continuously with the probe position ζ, while the phase can take on only two values during a measurement, differing by 180°, jumping from one value to the other at the zero passages. The 50 kHz signal is amplified by a low noise amplifier and reaches a lock-in amplifier (PSD) for converting the 50 kHz-signal into a corresponding dc-signal. High linearity and a dynamic range of about 100 dB is necessary here; it can be reached easily because the 50 kHz-phase remains constant. For comparison, the LF-phase varies continuously in the heterodyne system used in [14], leading to difficulties in voltage measurements with PSDs [14]. The dc-output signal of the PSD is called $V_{tot}(\zeta)$, cf. [15]. After A/D conversion (12 bit) the signal is stored in the memory of a Fabritec 1072 signal averager.

The probe system is shifted by a micrometer screw with 0.5 mm displacement per rotation, which is driven by a motor. In the X-Band, a total displacement of 35 mm can be reached. An optical device delivers 60 light pulses per micrometer revolution on a photodiode. These pulses trigger the external address advance of the Fabritec, resulting in a proper assignment of channel number and probe position ζ. The signal function $V_{tot}(\zeta_i)$ is transferred from the Fabritec memory to a PC (Atari 1040 ST). Data evaluation was executed on a Cyber 855.

The main physical difference between the homodyne system described here and the heterodyne system described in [13] is the fact that in the homodyne system the transfer of phase information is restricted to the microwave part of the system, which is highly linear and insensitive against leakages. Additionally, the use of two IF-mixers with their linearity problems (cf. below) and the complicated IF-structure described in [13] is avoided.

Temperature Measurements

The temperature was measured by a Cu-constantan thermocouple close to the sliding probe and moved with it in the sample liquid. Thermovoltages were measured with a 5½ digit Schlumberger solartron, resolution being 0.05 °C. Alternatively, a sensitive dc-amplifier was used, allowing measurements of tem-

perature gradients along the ζ-direction with 0.01 °C resolution. In the X-Band we used two combined thermostats. The thin waveguide R 500 of the X-Band is in good thermal contact with a heat exchange vessel made of brass, which is connected to a water circulating thermostat. This exchanger itself is mounted together with all the essential parts of the waveguide in a large (390 × 250 × 160 mm) tempered oil bath. The measured temperature gradients are smaller than 0.01 °C per 60 mm probe displacement at 45 °C. In the S-Band, the waveguide R 320 was embedded with thermally good contact in a heavy brass cylinder, which was tempered by a thermostat. Temperature gradients were smaller then 0.05 °C per 120 mm probe displacement.

Error Discussions

Diode Characteristic

As a basic assumption for linear detection [15, 17, 19] it must be demanded that

$$|U_R| \gg |U_S|. \tag{1}$$

To check this assumption, we introduce the quantity

$$\eta \equiv U_0/|U_R| = \max(|U_S|)/|U_R|. \tag{2}$$

Furthermore, the dc-output of the PSD is given by the function

$$V(\zeta_i) = f(|U_R + U_S|) - f(|U_R|), \tag{3}$$

where the function $f(U)$ contains the diode characteristic. The difference corresponds to switching the pin diode on and off. Assuming that only the TE_{01}-mode is measured, we get according to Fig. 1 (insert) of [15]

$$|U_S| = U_0 \exp(-K''\zeta_i), \quad \alpha = K'\zeta_i, \tag{4}$$

and

$$|U_R + U_S| = \sqrt{|U_R|^2 + |U_S|^2 - 2|U_R||U_S|\cos\alpha}$$
$$= |U_R|\sqrt{1 - 2\eta\exp(-K''\zeta_i)\cos(K'\zeta_i) + \eta^2\exp(-2K''\zeta_i)}. \tag{5}$$

Assuming first a quadratic crystal characteristic [19], the dc-output of the PSD yields

$$V = C_1(|U_R + U_S|^2 - |U_R|^2) \tag{6}$$

(cf. (3)). C_1 is a conversion constant. Combining (5) and (6), we get as modified function $V_m(\zeta_i)$ (cf. [15]):

$$V_m(\zeta_i) = -C_1 U_0 |U_R| \tag{7}$$
$$\cdot \{2\exp(-K''\zeta_i)\cos(K'\zeta_i) - \eta\exp(-2K''\zeta_i)\}.$$

The dc-output of the PSD is proportional to the reference voltage U_R and to the signal voltage U_0 in this case. Except for an arbitrary phase and amplitude offset Ψ_0 and V_0, (7) is identical with the basic equation (2) of [15] in the limit $\eta \ll 1$:

$$V(\zeta_i, X) = V_0 + V \sin((K'\zeta_i) + \Psi_0) \exp(-K''\zeta_i). \quad (8)$$

Deviations of (7) from (8) appear in the first order of η, independent of the phase angle $(K'\zeta_i)$. At high bias levels, where the diode characteristic is linear [19], the output of the PSD may be calculated with

$$V = C_2(|U_R + U_S| - |U_R|). \quad (9)$$

C_2 is the high level gain constant. Expansion of (5) into a power series and combination with (9) yields

$$V_m(\zeta_i) = -C_2 U_0 \{\exp(-K''\zeta_i)\cos(K'\zeta_i) \quad (10)$$
$$+ 1/2\eta \exp(-2K''\zeta_i)(\cos^2(K'\zeta_i) - 1)\}.$$

In this case, the deviation from (8) is due to the phase variation $(K'\zeta_i)$ (projection error). This deviation appears in first order of η too.

Fitting of (8) to measured curves $V_{tot}(\zeta_i)$ would lead to systematic errors for non-zero values of η. In the following we calculate these systematic errors for the case of linear detection, the operating condition of the systems used here. (The total linearity error of a high biased diode is by far less than 0.001 dB [19].) We calculate the function $V_m(\zeta_i)$, using (9) and (5), for both frequencies and literature values of ε^* for water. Then values of ε^* were calculated by fitting (8) to these simulated spectra.

In turned out that the errors in the interesting range $10^{-4} < \eta < 5 \cdot 10^{-2}$ are proportional to η; so the following definitions are senseful:

$$\Delta\varepsilon'/\varepsilon' = F'\eta, \quad \Delta\varepsilon''/\varepsilon'' = F''\eta. \quad (11)$$

F' and F'' are functions of ε', ε'', ω and the phase offset Ψ_0. We have found the relation

$$F(\Psi_0) \approx -F(\pi - \Psi_0). \quad (12)$$

The factors $F(\varepsilon', \varepsilon'', \omega, \Psi_0)$ have been evaluated from about 200 spectral simulations. To summarize, the inequality

$$|F| < 0.2 \quad (13)$$

holds for both frequencies.

Some results are shown in Table 1. In most of the cases corrections due to the projection error are in the ‰ range for $\eta = 1.9 \cdot 10^{-2}$ used here. This η-value cor-
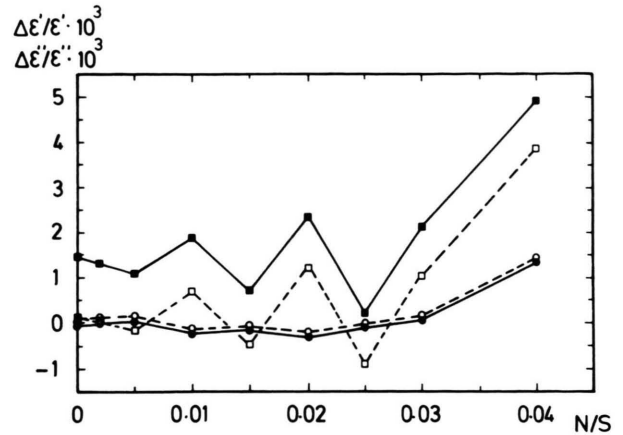

Fig. 3. Relative errors $\Delta\varepsilon'/\varepsilon'$ and $\Delta\varepsilon''/\varepsilon''$ as functions of the noise to signal ratio N/S for 2 different resolutions of the AD-converter: (●), $\Delta\varepsilon'/\varepsilon'$, 12 bit; (○), $\Delta\varepsilon'/\varepsilon'$, 16 bit; (■), $\Delta\varepsilon''/\varepsilon''$, 12 bit; (□), $\Delta\varepsilon''/\varepsilon''$, 16 bit.

Table 1. Errors in ε^*-values of water due to non-linearities of the homodyne mixing. Spectra are simulated using (10) as modified function ($\eta = 1.9 \cdot 10^{-2}$) and are fitted using (8). From these values the resp. F' and F'' values according to (11) can be calculated.

$T/°C$	9.376 GHz		3.587 GHz	
	$\dfrac{\Delta\varepsilon'/\varepsilon'}{10^{-3}}$	$\dfrac{\Delta\varepsilon''/\varepsilon''}{10^{-3}}$	$\dfrac{\Delta\varepsilon'/\varepsilon'}{10^{-3}}$	$\dfrac{\Delta\varepsilon''/\varepsilon''}{10^{-3}}$
10	−4.7	−2.7	−1.7	<0.1
20	−3.5	−1.2	−1.1	0.6
30	−2.6	−0.08	−0.7	1.0
40	−1.8	0.7	−0.5	1.4

responds to that used in heterodyne mixing described in [13] and was used in [10–12] without corrections. It should be stressed that nowadays set-ups can be realized that allow measurements with good signal to noise ratio with $\eta = 2 \cdot 10^{-3}$. In these cases the simple equation (8) can be used for data evaluation, and the total systematic non-linearity errors are less than 0.3‰ (cf. Table 1).

The ε^*-values of water, given in this paper, have been calculated from the experimental spectra using (10) (or the not expanded combination of (5) and (9)). Thus we avoided the systematic non-linearity errors completely.

We conclude that the important systematic error source, resulting from the violation of the basic equation (1), can be calculated or made negligibly small for homodyne systems. Comparing the methods again, it turns out that the linearity of the homodyne mixing is
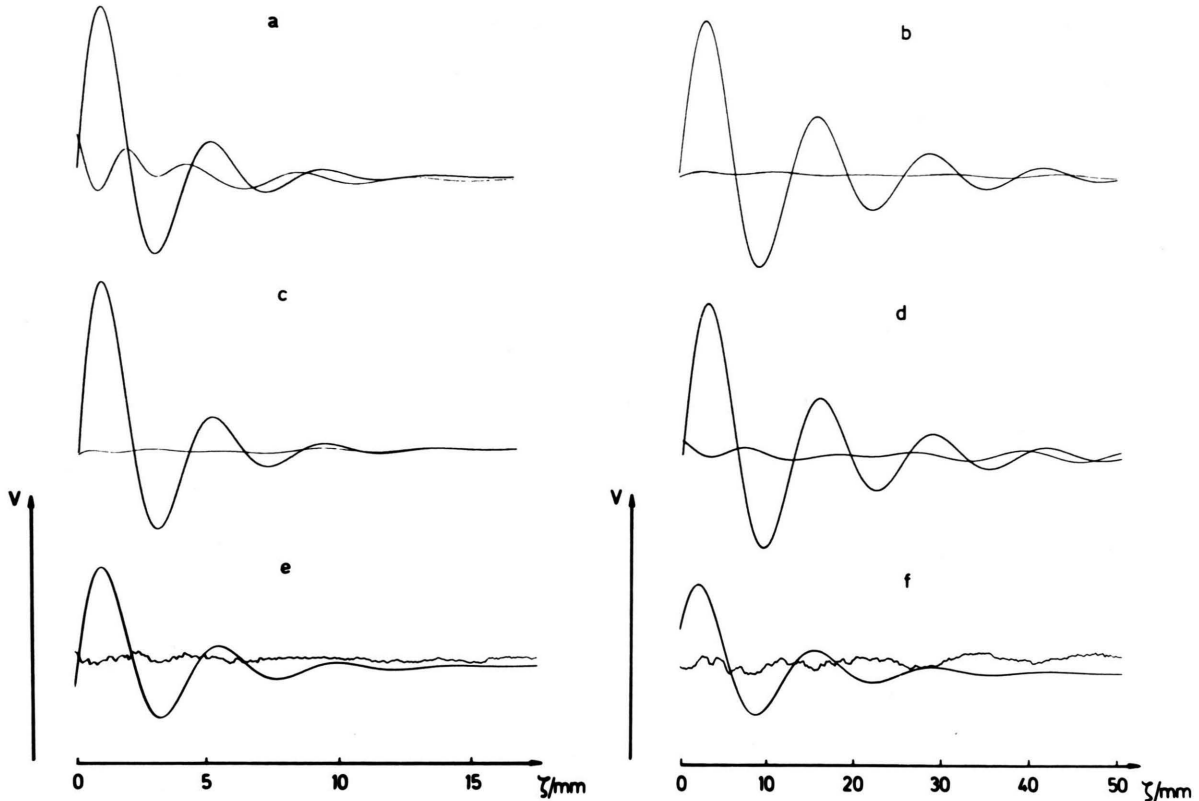
Fig. 4. Signal voltage V as function of the probe position for 9.376 GHz (left) and 3.587 GHz (right). (a) Diode characteristic (projection error): Fit of the basic equation (8) to a simulation of V according to (10), $\eta = 1.9 \cdot 10^{-2}$, ε^* values correspond to the values of water at 25 °C. The simulation and the difference plot ($\cdot$ 50) between simulation and fit according to [15], Eq. (5), are shown. In the ε^* measurements discussed later, this error source is avoided by fitting (10) instead of (8) to the measured spectra. (b, c) Temperature gradient: Fits of (8) to simulations of V according to (17). The assumed temperature gradient is $5 \cdot 10^{-3}$ K/mm for 3.6 GHz and $5 \cdot 10^{-2}$ K/mm for 9.3 GHz. (The experimental temperature gradient is less than $5 \cdot 10^{-4}$ K/mm.) ε^* values and the temperature dependence of ε^* for water (25 °C) are chosen for the simulation. (d) Waveguide surface quality: Fits of (8) to simulations of V using (19) with $K_c(\zeta)$ corresponding to the experimental waveguide dimensions $a(\zeta)$. The simulation and the difference between simulation and fit are shown. (e, f) Experimental signal voltage V_{tot} and difference between measurement and fit. Comparing this difference plot with those of different error sources given in (b)–(d), we conclude that the observed deviation is due to the surface roughness of the waveguide.

superior compared to the heterodyne system's linearity [19].

As a tool to find additional possible errors sources we have compared spectra, in which a systematic error is simulated, with spectra of the usual form (8). The difference of these spectra is in many cases typical for a certain type of error. Examples are discussed in the following section, difference plots are given in Figure 4.

Amplifier- and Converter Noise

We simulate these two error sources together and choose as a modified function

$$V_m(\zeta_i) = [S \exp(-K'' \zeta_i) \sin(K' \zeta_i + \Psi_0) + N \cdot Z_j(\zeta_i)] \,. \quad (14)$$

Here the bracket [ ] means an integer function. Corresponding to the two A/D converters to be compared (12 and 16 bit resolution) S has values of 2^{11} and 2^{15}, respectively. Electronic noise is simulated additionally by random numbers $Z_j(\zeta_i)$, where

$$-1 \leqq Z_j(\zeta_i) \leqq 1 \,.$$

The index j characterizes the sequence of random numbers completely (see below). S/N is the maximum signal to noise ratio. Using the method described in [15], we get two corresponding errors $\Delta\varepsilon'/\varepsilon'$ and $\Delta\varepsilon''/\varepsilon''$ for every triple $(S, j, S/N)$.

To reduce the influence of a special sequence of random numbers, we average over 10 simulations,

which are characterized by the index j. So we get

$$\Delta\varepsilon'/\varepsilon'(S, S/N) = 1/10 \sum_{j=1}^{10} \Delta\varepsilon'/\varepsilon'(S, j, S/N),$$

$$\Delta\varepsilon''/\varepsilon''(S, S/N) = 1/10 \sum_{j=1}^{10} \Delta\varepsilon''/\varepsilon''(S, j, S/N). \quad (15)$$

Errors calculated for 10 values of S/N with $S = 2^{11}$ and $S = 2^{15}$ (realized by 200 fits) for ε^* values corresponding to water for $T = 25\,°C$ and $f = 9.356\,GHz$ are shown in Figure 3.

With a 12 bit converter and $N/S < 5 \cdot 10^{-3}$, we will find errors up to 1‰. As the calculations show, $\Delta\varepsilon''/\varepsilon''$ is always positiv in this N/S-range. That means, the ε''-errors shown in Fig. 3 for 12 bit converters in the limit $N/S = 0$ are systematic erros. It should be mentioned that an 11 bit converter is used in [10] and [11], a 12 bit converter in this work, and a 14 bit in [12]. With a 16 bit converter, no systematic errors in the ‰ range occur, if $N/S < 3 \cdot 10^{-2}$.

The systematic errors on the measurements of ε' and ε'', caused by the 12 bit converter used in this work, were not corrected.

Temperature Gradient Errors

Errors of 0.05 °C in temperature lead to errors of 0.8‰ in ε' and ε'', if we take the ε^* values of water for 10 °C, where the temperature dependence of ε^* is high.

To simulate the effect of temperature gradients in the direction of the probe displacement, we assume approximately a linear dependence

$$T(\zeta) = T_0 + dT/d\zeta \cdot \zeta. \quad (16)$$

The influence of the temperature gradient on the propagation of the microwave is simulated in the following way: The gradient leads to a local variation of the dielectric constant $\varepsilon^*(T(\zeta))$. The temperature dependence of ε^* of water being well known, we calculate the dependence of the propagation constant $K^*(T(\zeta))$ on ζ. As an approximation, we use as the modified function

$$V_m(\zeta_{i+1}) = a_{i+1} \sin \phi_{i+1},$$

where

$$a_1 = V_0,$$
$$a_{i+1} = a_i \exp(-K''(\zeta_i)\,\delta\zeta), \quad (17)$$
$$\phi_{i+1} = \phi_i + K'(\zeta_i)\,\delta\zeta,$$
$$\delta\zeta = \zeta_{i+1} - \zeta_i.$$

This procedure is justified if the relative change of K^* over the distance $\delta\zeta$ is sufficiently small.

After this, we proceed as described, calculate the systematic errors and find in a good approximation that

$$\Delta\varepsilon'/\varepsilon' \approx a(\Delta T/\Delta z) \quad \text{and} \quad \Delta\varepsilon''/\varepsilon'' \approx b(\Delta T/\Delta z) \quad (18)$$

with

RG 500:
$a = -0.026\,mm/K, \quad b = 0.095\,mm/K$ for 9.376 GHz,

RG 320:
$a = 0.038\,mm/K, \quad b = 0.280\,mm/K$ for 3.587 GHz

for water of 25 °C and gradients of less than 0.1 K/mm. In the experiments, temperature gradients were found to be less than $5 \cdot 10^{-4}$ K/mm. These gradients gave neither visible difference plots nor critical systematic errors (cf. Fig. 4 b, c).

Waveguide Surface Quality

The accuracy limiting factor in all ε^* measurements reported here is given by the surface quality of the waveguide used. Since the broad dimension a of the waveguide determines the cutoff constant $K_c = \pi/a$ and therefore K^*, a local roughness with suitable length and intensity causes systematic errors in ε^*. To check this error source, we first measured $a(\zeta_i) = a_0 + \Delta a(\zeta_i)$ with a capacitive plunger of 15 mm length in the empty waveguide using an LF-method. A result for R 320 shows a surface structure of 10^{-2} mm over a range of 80 mm length, which was exactly reproducible. Using $K_c(\zeta_i) = \pi/(a_0 + \Delta a(\zeta_i))$ and known values of ε^* (water, 25°, 3.6 GHz) we calculated $K^*(\zeta_i)$ for the water filled waveguide R 320 according to the measured surface roughness. Using these values of $K^*(\zeta_i)$, we get as the modified function

$$V_m(\zeta_{i+1}) = a_{i+1} \sin \phi_{i+1},$$

where

$$a_1 = V_0,$$
$$a_{i+1} = a_i \exp(-K''(\zeta_i)\,\delta\zeta), \quad (19)$$
$$\phi_{i+1} = \phi_i + K'(\zeta_i)\,\delta\zeta,$$
$$\delta\zeta = \zeta_{i+1} - \zeta_i.$$

(We note, that (19) has the same shape as (17) used for temperature gradient discussion.) Using (19), we cal-

culate difference plots and ε*-errors, as described. The errors corresponding to the difference plot shown in Fig. 4 d are $\Delta\varepsilon'/\varepsilon' = 0.2‰$ and $\Delta\varepsilon''/\varepsilon'' = 0.3‰$. We compare these difference plots with typical experimental difference plots and find good consistency.

Furthermore, the curvature of the waveguide walls causes deflections of the sliding copper block which supports the coupling loop (cf. Figure 2). The resulting lateral deflections of the coupling loop from its centre position lead to fluctuations of the sensed amplitude of the local H-field. The resulting noise structure is proportional to the signal strength.

Typical measuring spectra and difference plots between measurement and fit for 9.376 GHz and 3.587 GHz are shown in Fig. 4 e, f. We recognize differences between measurement and fit due to the two distortion mechanisms discussed above: A noise structure which decreases with decreasing signal strength due to the probe fluctuations, and a ripple according to the fluctuation of the cutoff constant of the waveguide. In the following experiments the ε*-measurements were done in waveguide sections, where the typical difference plots were as weak as possible. The remaining errors (1‰ in ε' and 1.5‰ in ε') are not corrected in this work.

Measurements on Water

Numerical Results

Measurements were carried out on quartz destilled water in the temperature range 6 °C–45 °C at 9.376 and 3.587 GHz.

The results are given as polynomials of third order, T in °C,

$$\varepsilon = a_0 + a_1 T + a_2 T^2 + a_3 T^3. \tag{20}$$

Table 2 shows the coefficients of the polynomial fits together with the standard deviations of these fits. The

accuracy, however, is determined by the systematic error source already discussed, which is not corrected here (waveguide surface quality). For comparison, the coefficients given in [12] are shown, which are directly comparable with those found in our work. The frequency difference of 2‰ leads to maximum errors of 1.3‰ in ε' and 1.7‰ in ε''. The maximum deviations between the values given in [12] and this work are $\Delta\varepsilon' = -6.9‰$ and $\Delta\varepsilon'' = 16.7‰$ (40 °C).

Figure 5 shows the experimental results at two frequencies. Each ε* value is the mean taken from about 6 single measurements. The standard deviation of the mean value is less than 0.085 for ε' and 0.06 for ε'' in all cases.
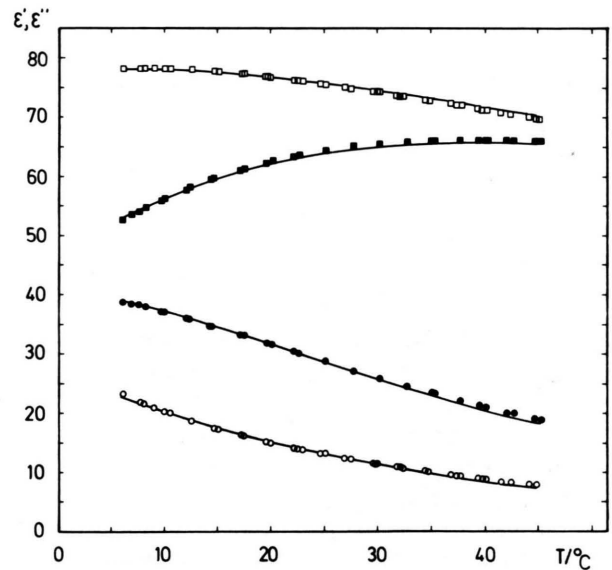

Fig. 5. ε*-values of water for two frequencies vs. temperature. (■), ε', 9.376 GHz; (□), ε' for 3.587 GHz; (●), ε'', 9.376 GHz; (○), ε'', 3.587 GHz. The curves are fits of (21)–(23) to the complete set of experimental data points with the relaxation parameters given in Table 4, column 2 (4 parameter Cole fit).

Table 2. Coefficients of the polynomial fits, (20).

	v/GHz	T/°C	a_0	a_1	a_2	a_3	σ
ε'	9.376	6–45	45.588	1.3119	−0.0267	0.000170	0.064
ε' *	9.356	10–40	44.73	1.430	−0.0318	0.000230	0.036
ε''	9.376	6–45	41.281	−0.3356	−0.0102	0.000151	0.093
ε'' *	9.356	10–40	41.96	−0.407	−0.0083	0.000132	0.035
ε'	3.587	6–45	77.620	0.1802	−0.0137	0.000131	0.073
ε''	3.587	6–45	28.554	−0.9833	0.0182	−0.000147	0.086

* Values are taken from [12].

Table 3. Fits of (21) (Cole equation) to ε' and ε'' at 9.376 GHz.

Parameters	3	4	5	6
$\ln(h/k) - \Delta S/R$	-26.55 ± 0.06 (-26.51 ± 0.04)	-25.97 ± 0.06 (-26.38 ± 0.08)	-26.28 ± 0.15 (-26.22 ± 0.22)	-33.56 ± 0.50 (-34.39 ± 0.57)
$\Delta H/\text{kJ mol}^{-1}$	16.62 ± 0.15 (16.53 ± 0.10)	15.50 ± 0.13 (16.28 ± 0.15)	16.09 ± 0.29 (15.98 ± 0.42)	32.26 ± 1.08 (34.10 ± 1.23)
ε_∞	3.47 ± 0.29 (3.89 ± 0.16)	10.92 ± 0.64 (5.73 ± 0.87)	6.75 ± 2.11 (7.97 ± 2.96)	-41.6 ± 4.4 (-46.64 ± 5.16)
α	$-$ $(-)$	-0.0284 ± 0.037 (0.0032 ± 0.0042)	0.0003 ± 0.0135 (-0.011 ± 0.02)	0.41 ± 0.02 (0.43 ± 0.02)
b	$-$ $(-)$	$-$ $(-)$	-0.0044 ± 0.00010 (-0.0047 ± 0.00013)	-0.0082 ± 0.0002 (-0.0088 ± 0.0002)
ε_s (0 °C)	$-$ $(-)$	$-$ $(-)$	$-$ $(-)$	124.4 ± 2.5 (127.4 ± 2.7)
σ_tot	0.372 (0.149)	0.206 (0.142)	0.198 (0.142)	0.102 (0.059)

The values in brackets are the parameters calculated from the experimental ε^* values given in [12]. The bars indicate the parameters which are held fixed: $\alpha = 0.012$, $b = -0.00458$, $\varepsilon_\text{s}(0\,°\text{C}) = 87.83$ [20], $\sigma_\text{tot} = (Q/(N-n_x))^{1/2}$. Q and N are defined in (24), n_x is the number of fit parameters.

Determination of the Relaxation Parameters

To describe the water relaxation we use the Cole-equation [5, 4]

$$\varepsilon^* = \varepsilon_\infty + (\varepsilon_\text{s} - \varepsilon_\infty)/(1 + (i\,\omega\,\tau)^{1-\alpha}). \tag{21}$$

To couple the ε^* values of different temperatures, we used the expressions [12, 20, 21]

$$\varepsilon_\text{s}(T) = \varepsilon_\text{s}(0\,°\text{C}) \exp(b\,T), \tag{22}$$

$$\tau(T) = h/kT \exp(-\Delta H/RT) \exp(-\Delta S/R). \tag{23}$$

So the temperature and frequency dependencies of the water relaxation can be described by 6 parameters: ΔS, ΔH, ε_∞, α, b, and ε_s (0 °C).

To calculate these parameters, the experimental values $\varepsilon^*_\text{meas}(\omega, T)$ have to be compared with values $\varepsilon^*_\text{cole}(\omega, T)$ which are calculated using (21)–(23) with a suitable set of the six parameters mentioned. We have to minimize the function

$$Q(x) = \sum_{i=1}^{N} |\varepsilon^*_\text{meas}(\omega, T_i) - \varepsilon^*_\text{cole}(\omega, T_i, x)|^2 \tag{24}$$

to find the optimum parameter vector x (ΔS; ΔH; ε_∞; $\varepsilon_\text{s}(0\,°\text{C})$, α, b) (least squares fitting [24]). N is the number of measurement values used.

Table 3 shows the values we calculated from our measurements at 9.376 GHz. For comparison the values in brackets are calculated from the experimental ε^*-values given in [12]. In the head of each column the number of fit parameters is given. Those parameters, which are fixed on this respective fit, are indicated by

bars. The values which were assumed for these fixed parameters are given in the legend. The total standard deviation σ_tot of the whole fit is given, too.

The following statements hold for the results from both data sets: The standard deviation σ for any single parameter drastically increases with increasing number of free running fit parameters, while σ_tot decreases. This indicates a strong correlation between these parameters. In the Cole-fit with 6 fit parameters (column 4), unphysical values appear for all parameters together with high σ-values, but σ_tot is very low. That means that the total fit is excellent but the parameters calculated are wrong. Furthermore, we note that the evaluation of the six parameters from the ε^*-values given in [12] leads here to other values (values in brackets) than the values given in [12]: Good values for the relaxation parameters are given in [12], whereas unphysical values (Table 3, column 4) are calculated here. It should be stressed that the values in Table 3 are reached also with starting values very close to the "physical" set of these parameters. We don't have any explanation for this.

Due to the correlation between the parameters it is possible to describe the experimental result with different solution vectors. The problem increases if only $\varepsilon'(T)$ or $\varepsilon''(T)$ alone is used for the calculation. Using $\varepsilon'(T)$-values calculated from (21) with a suitable parameter vector, we found that only the first 4 of the 6 parameters could be fitted back with certainty. If calculated $\varepsilon''(T)$-values are used, only 3 parameters could be determined authenticly.

Table 4. Fits of (21) to ε' and ε'' for 9.356 and 3.587 GHz.

Parameters	3 (Cole)	4 (Cole)	6 (Cole)	5 (Debye)
$\ln(h/k) - \Delta S/R$	-26.48 ± 0.05	-26.37 ± 0.06	-26.27 ± 0.06	-26.36 ± 0.05
$\Delta H/\text{kJ mol}^{-1}$	16.45 ± 0.12	16.24 ± 0.13	16.06 ± 0.14	16.22 ± 0.11
ε_∞	3.39 ± 0.27	5.22 ± 0.57	6.32 ± 0.58	5.33 ± 0.33
α	–	0.0035 ± 0.0024	-0.0073 ± 0.0036	–
b	–	–	-0.00462 ± 0.00005	-0.00463 ± 0.00005
$\varepsilon_s(0\,^\circ\text{C})$	–	–	87.55 ± 0.16	87.73 ± 0.13
σ_{tot}	0.354	0.339	0.321	0.325

The parameters were calculated using 29 experimental values of ε^* at 9.356 GHz and 39 values of ε^* at 3.587 GHz. Each value includes in the mean six single measurements at the same temperature with typical standard deviations of 0.08 and 0.1 for ε' and ε'', respectively, at 9.376 GHz, and 0.02 and 0.035, respectively, at 3.587 GHz. The values of the fixed parameters (indicated by bars) are given in the legend of Table 3.

Difficulties do not appear if the results determined at 9.4 and 3.6 GHz are used together. Here we have to minimize the function

$$Q(x) = \sum_{i=1}^{N_1} |\varepsilon^*_{\text{meas}}(\omega_1, T_i) - \varepsilon^*_{\text{cole}}(\omega_1, T_i, x)|^2$$
$$+ \sum_{i=1}^{N_2} |\varepsilon^*_{\text{meas}}(\omega_2, T_i) - \varepsilon^*_{\text{cole}}(\omega_2, T_i, x)|^2 \quad (25)$$

instead of (24). The results of the fittings are summarized in Table 4. For most of the parameters we do not find a standard deviation which increases with increasing number of fit-parameters – in contrast to the results for one frequency. It seems that the correlation between the relaxation parameters is less in this case. The determination of all 5 parameters of the Debye function ($\alpha = 0$) is possible. Additionally the determination of the distribution parameter α [22] is possible, if literature values of $\varepsilon_s(T) = \varepsilon_s(0\,^\circ\text{C}) \exp(bT)$ are used. The results summarized in Tables 3 and 4 give examples of the numerical coupling of α and ε_∞, as already mentioned by Grant et al. [8]. It is difficult to determine both quantities together; so the standard deviation of ε_∞ increases in the 4-parameter fit, and unphysical negative values of α appear if 5 or 6 parameters are fitted. On the other hand, the determination of $\Delta G = \Delta H - T\Delta S$ and $\varepsilon_s(T)$ is possible with very high accuracy even from the 6-parameter-Cole-fit. The result of the fittings of the first 4 parameters to the experimental values of both frequencies is shown in Figure 5.

The Dependence of the Kinetic Parameters on the Relaxation Model

An independent low-frequency determination of $\varepsilon_s(T)$ is possible with outstanding accuracy. Therefore $\varepsilon_s(T)$ is ideal as a reference quantity, as done in the 3 and 4 parameter-Cole-fit listed in Table 4. The temperature dependence of the relaxation time function $\tau(T)$ is model dependent. Equation (23) expresses the Eyring model of dielectric relaxation [23], while other relations like

$$\tau_B = h/kT_0 \exp(-\Delta S/R) \exp(\Delta H/RT), \quad (26)$$

$$\tau_C = h/(k\sqrt{(T/T_0)}) \exp(-\Delta S/R) \exp(\Delta H/RT), \quad (27)$$

are in use, too, as mentioned in [16]. T_0 is a fixed temperature. We investigated the consequences of the use of (26) or (27) instead of (23) by model calculations. For this we calculated first $\varepsilon^*(T)$ values for water, using (21) and (23) with the following parameters:

$$\ln(h/k) - \Delta S/k = -26.48,$$
$$\Delta H = 16.45\ \text{kJ/mol},$$
$$\varepsilon_\infty = 3.4,$$
$$\alpha = 0.012,$$
$$b = -0.00458,$$
$$\varepsilon_s(0\,^\circ\text{C}) = 87.83$$

for a frequency of 9.376 GHz in the temperature range $6\,^\circ\text{C} - 45\,^\circ\text{C}$. These calculated values $\varepsilon^*(T)$ were then fitted again with (21), using (26) or alternatively (27) as expression for τ instead of (23). For these fits, the relaxation parameters α, b, $\varepsilon_s(0\,^\circ\text{C})$ and ω were fixed at the values given above, while ε_∞, ΔS and ΔH are fitted. To demonstrate the coupling effect mentioned above, we used different data sets, namely $\varepsilon'(T)$ alone, $\varepsilon''(T)$ alone, $\varepsilon'(T)$ and $\varepsilon''(T)$ together. The results are
– Fitting $\varepsilon'(T)$ or $\varepsilon''(T)$:
We find very different ε_∞-values ($3.5 < \varepsilon_\infty < 5.7$) with very low σ-values ($\sigma < 0.002$) corresponding to the different relaxation models (26) and (27). A similar result has already been observed in fitting the

experimental ε-values (cf. Table 3). This is physically not realistic.

- Fitting the data set $\varepsilon'(T)$ and $\varepsilon''(T)$:
  ε_∞ differs only at the 0.001 level (and is identical with the starting value assumed above) for the different models (26), (27). The model dependency is now expressed in ΔH, which is reasonable. The models (23), (26) and (27) have ΔH-values of $\Delta H = 16.45$ kJ/ mol, 17.68 kJ/mol, and 18.91 kJ/mol respectively.

- All fits were finished after 4, sometimes 5 steps corresponding to the self adjusting gradient length used here [24, 25]. The same step number holds for

fitting the experimental data, where σ-values are up to 50 times larger.

We conclude from these model calculations that the ΔH-values, even if determined with a broad data set, have a residual uncertainty of about 20%, which is due to the underlying physical relaxation model.

[1] R. Pottel, K. Giese, and U. Kaatze, in: Structure of Water and Aqueous Solutions (W. A. P. Luck, ed.), pp. 392–407, Verlag Chemie, Weinheim 1974.
[2] J. B. Hasted, in: Water, A Comprehensive Treatise, Vol. 1, The Physics and Physical Chemistry of Water (F. Franks, ed.), pp. 255–309, Plenum Press, New York 1972.
[3] J. B. Hasted (ed.), Aqueous Dielectrics, Chapmann and Hall, London 1973.
[4] U. Kaatze and V. Uhlendorf, Z. Phys. Chemie, N.F. **126**, 151 (1981).
[5] K. S. Cole and R. H. Cole, J. Chem. Phys. **9**, 341 (1941).
[6] N. E. Hill, J. Phys. C **3**, 238 (1970).
[7] N. E. Hill, Trans. Faraday Soc. **59**, 344 (1963).
[8] E. H. Grant and R. Shack, Brit. J. Appl. Phys. **18**, 1807 (1967).
[9] J. B. Hasted, S. K. Husain, F. A. Frescura, and J. R. Birch, Infrared Physics **27**, 11 (1987).
[10] J. G. McAvoy and H. A. Buckmaster, J. Phys. D **16**, 2519 (1983).
[11] J. G. McAvoy and H. A. Buckmaster, J. Phys. D **17**, 2081 (1984).
[12] H. Zaghloul and H. A. Buckmaster, J. Phys. D **18**, 2109 (1985).
[13] J. G. McAvoy and H. A. Buckmaster, J. Phys. E **18**, 244 (1985).
[14] T. H. T. Van Kalleveen and H. A. Buckmaster, Can. J. Chem. **66**, 672 (1988).
[15] A. Redhardt, H. J. Steinhoff, J. Schlitter, H. J,. Neumann, and G. Hess, Z. Naturforsch. **44a**, 75 (1989).
[16] E. H. Grant, R. J. Sheppard, and G. P. South, Dielectric Behaviour of Biological Molecules in Solution, Clarendon Press, London 1978.
[17] A. Redhardt and W. Daseler, J. Biochem. Biophys. Methods **15**, 71 (1987).
[18] R. J. Sheppard, J. Phys. D **5**, 1576 (1972).
[19] R. J. King, Microwave Homodyne Techniques (Peregrinus, ed.), Stevenage 1978.
[20] G. A. Vidulich, D. F. Evans, and R. L. Kay, J. Phys. Chem. **71**, 656 (1967).
[21] K. E. Larssen and U. Dahlberg, Reactor Sci. Technol. (J. Nucl. Eng.) **16**, 81 (1965).
[22] H. P. Schwan, Z. Naturforsch. **9a**, 35 (1954).
[23] W. Kauzmann, Rev. Mod. Phys. **14**, 12 (1942).
[24] D. Braess, Computing **1**, 264 (1966).
[25] P. R. Levington, Data Reduction and Error Analysis for the Physical Sciences, McGraw-Hill, New York 1969.